# NUMERICAL SIMULATION AND EXPERIMENTAL VALIDATION OF WIRE ARC ADDITIVE MANUFACTURING OF PURE COPPER

**MTech Thesis**

By
**Bhavesh Jain**
**(2102103005)**

**DISCIPLINE OF MECHANICAL ENGINEERING**
**INDIAN INSTITUTE OF TECHNOLOGY INDORE**

**JUNE 2023**

# NUMERICAL SIMULATION AND EXPERIMENTAL VALIDATION OF WIRE ARC ADDITIVE MANUFACTURING OF PURE COPPER

**A THESIS**

*Submitted in partial fulfillment of the requirements for the award of the degree*

***of***

**Master of Technology**

*by*


**BHAVESH JAIN**



**DISCIPLINE OF MECHANICAL ENGINEERING**

**INDIAN INSTITUTE OF TECHNOLOGY INDORE**


**JUNE 2023**

# INDIAN INSTITUTE OF TECHNOLOGY INDORE

## CANDIDATE'S DECLARATION

I hereby certify that the work which is being presented in the thesis entitled **NUMERICAL SIMULATION AND EXPERIMENTAL VALIDATION OF WIRE ARC ADDITIVE MANUFACTURING OF PURE COPPER** in the partial fulfillment of the requirements for the award of the degree of **MASTER OF TECHNOLOGY** and submitted in the **DISCIPLINE OFMECHANICAL ENGINEERING, Indian Institute of Technology Indore**, is an authentic record of my own work carried out during the time period from May 2022 to June 2023 under the supervision of **Dr. Dan Sathiaraj**, Assistant Professor, Department of Mechanical Engineering, Indian Institute of Technology, Indore.

The matter presented in this thesis has not been submitted by me for the award of any other degree of this or any other institute.

04/06/23

**Signature of the student with date**
**BHAVESH JAIN**

---

This is to certify that the above statement made by the candidate is correct to the best of my/our knowledge.

05.06.23

Signature of the Supervisor
**Dr. Dan Sathiaraj**

---

**Bhavesh Jain** has successfully given his/her M.Tech. Oral Examination held on **26 May 2023**.

Signature(s) of Supervisor(s) of M.Tech. thesis
Date: 05.06.2023

Convener, DPGC
Date: 06.06.2023

Signature of PSPC Member
**Dr. Yuvraj Kumar Madhukar**
Date: 06.06.2023

Signature of PSPC Member
**Dr. Abhijit Ghosh**
Date:06.06.2023

---

# ACKNOWLEDGEMENT

I would like to take this opportunity to convey my utmost respect and gratitude to **Dr. Dan Sathiaraj** for his unwavering belief in me and for providing me with this invaluable opportunity to work under his supervision. I am truly grateful for his consistent encouragement, amicable interactions, and constructive support, all of which have played a pivotal role in shaping the current state of this work. His innovative perspective and unwavering pursuit of perfection have had a profound impact on me, leading to significant personal transformation.

I extend my sincere appreciation to my PSPC members, **Dr. Yuvraj Kumar Madhukar,** and **Dr. Abhijit Ghosh**, for their invaluable guidance and support. Their active interest in my research and insightful discussions have fostered a deep exploration of my subject matter and have been instrumental in bringing this research to its present form.

I am grateful to IIT Indore for granting me permission to conduct this research and for providing the necessary facilities. I would like to acknowledge the **Head of Department of Mechanical Engineering** and the **DPGC convener** for their assistance, facilities, moral support, and kindness throughout my MTech program. I am indebted to **Miss Poonam Suresh Deshmukh** and **Mr. Rajendra Goud** for their invaluable assistance and guidance. I am truly grateful for the countless hours they dedicated to reviewing my work, providing constructive feedback, and sharing their extensive knowledge. I would also like to express my appreciation for the collaborative environment fostered by my seniors. Their willingness to engage in meaningful discussions and share their perspectives has enriched my research experience and broadened my horizons. I would also like to thank the **Laser Material Processing lab (LMP)** at IIT Indore for their assistance with the experimental work. My thanks also go to **Mr. Anas Ullah Khan** and **Mr. Atluri Bharath Kumar** for their support.

With Regards

**Bhavesh Jain**

# DEDICATION

*This thesis is dedicated to my parents, who have always encouraged me to pursue my dreams and instilled in me the value of knowledge and perseverance throughout my life.*

# ABSTRACT

Copper, known for its exceptional electrical and thermal conductivity, holds great potential for various industries. WAAM offers high deposition rates and the capability to manufacture intricate components. Nevertheless, during the WAAM process, continuous heat transfer to the workpiece and substrate can lead to the development of significant residual stresses within the component. To address this issue, preheating the substrate has proven effective in mitigating the formation of excessive residual stresses. In this study, copper bulk deposition is performed on both a substrate preheated to 300℃ and a non-preheated base plate. The two samples are subjected to subsequent mechanical and microstructural characterization to compare them. The preheated sample exhibits improvements in various aspects compared to the non-preheated sample. Specifically, the preheated sample demonstrates higher UTS of 280 MPa compared to 225 MPa in the non-preheated sample, increased hardness along the scanning direction (92 HV compared to 85 HV), and a higher coefficient of friction along the building direction (0.27 compared to 0.18) when compared to the non-preheated sample. Numerical models have also been developed to predict temperature profiles and induced residual stresses in the component. The simulation results are then verified against experimental data, and a strong agreement is observed between the two.

# LIST OF FIGURES

# LIST OF TABLES

# TABLE OF CONTENTS

# ABBREVIATIONS

| | |
|---|---|
| AM | Additive manufacturing |
| WAAM | Wire arc additive manufacturing |
| WEDM | Wire electric discharge machine |
| SEM | Scanning electron microscope |
| XRD | X-ray Diffraction |
| SLM | Selective Laser Melting |
| MIG | Metal inert gas |

# Chapter 1: INTRODUCTION

## 1.1 Additive Manufacturing:

Additive manufacturing (AM) is the advanced manufacturing technique that forms the final component by stacking layers of raw materials one upon another. It is a layer-by-layer manufacturing method. This technology is gaining huge attention owing to its advantages of high material utilization, lower cost, and capability of producing complex geometry. The feature of layer-by-layer deposition saves material and reduces processing cycle. There is no need for external tooling e.g., moulds, fixtures, dies and other complex process requirements of traditional manufacturing methods [1].

### *1.1.1 Classification of AM processes:*

The below classification of AM process (shown in Figure 1) is based on the different methods or techniques used for adding layers of material to create a 3D object:

**Material extrusion:** Also known as Fused Deposition Modelling (FDM), this additive manufacturing process involves the deposition of melted material through a nozzle or extruder. Commonly used materials include thermoplastics, waxes, and metals.

**Vat photopolymerization:** This process uses a vat of liquid photopolymer resin that is cured layer by layer using a UV light. It is commonly used for creating highly detailed objects, such as dental and jewellery models.

**Binder jetting**: This process involves the deposition of a binder onto a powder bed layer by layer. The binder acts as an adhesive, bonding the powder together to create a solid object. Binder jetting is commonly used for creating metal, ceramic, and sand moulds for casting.

**Powder bed fusion:** This type of additive manufacturing involves melting or sintering powdered material, such as metal, ceramic, or polymer, layer by layer using a laser or electron beam. Examples include selective laser sintering (SLS), direct metal laser sintering (DMLS), and electron beam melting (EBM).

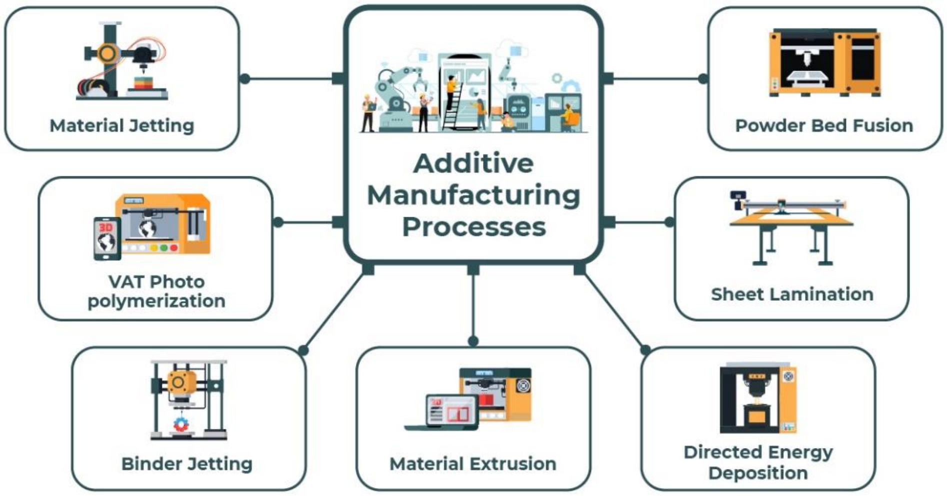


Figure 1 Classification of AM processes [23]

**Directed energy deposition:** This process involves the deposition of melted material through a nozzle onto a substrate. It is commonly used for repairing or adding material to an existing part or for creating new parts from scratch. Examples include laser engineered net shaping (LENS) and direct energy deposition (DED).

**Material Jetting:** This type of additive manufacturing uses an inkjet printer to deposit droplets of material layer by layer. It is commonly used for printing multi-material objects, such as those with varying colors or densities. Examples include polyjet and binder jetting.

## 1.2 Wire Arc Additive Manufacturing (WAAM):

Wire arc additive manufacturing (WAAM) is a metal additive manufacturing process that uses an electric arc to melt a wire feedstock and deposit it layer by layer to build up a 3D object. The wire is fed continuously into the arc, which melts the wire and deposits it onto the workpiece.

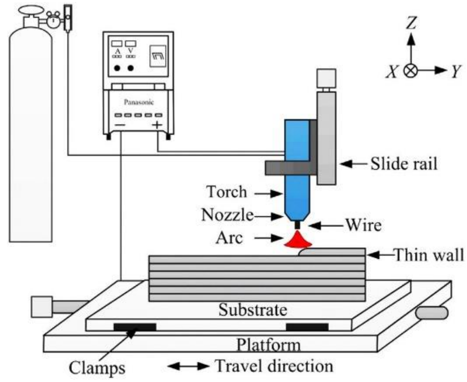


Figure 2: Schematic of WAAM process [24]

The wire itself acts as the electrode in this process. The shielding gas is also used to prevent oxidation during the deposition, generally inert gases like Argon (Ar) are used as shielding gases with optimum gas flow rate in this deposition process.

### *1.2.1 Advantages of WAAM process:*

Using the WAAM technique, 3D components may be produced with more freedom. There is no need for external machine equipment, dies, or casting molds [1]. With a rapid deposition rate and minimal material waste, this WAAM method has a very high degree of feed material utilization. When manufacturing complicated parts or components, less material waste might result in lower potential costs and shorter lead times[1]. The Layer-by-layer deposition characteristics is used to create complex parts and preforms of medium and large sizes that are close to net shapes. Moreover, the generated part is accurate and has a superior surface polish.

### *1.2.3 Disadvantages of WAAM:*

The heat generated is relatively high compared to other additive manufacturing processes, generating residual strains and distortions in the finished component [2]. Also, the complex part production can be considered to have a lower level of surface polish. In some circumstances, the operator's competence and ongoing observation are necessary for a successful build-up of layers; otherwise, cracks may emerge. Moreover, to get rid of splatter and extra material on the substrate, post finishing processes are carried out.

## 1.3 Pure copper and its applications:


Figure 3 Applications of pure copper [25]

The combination of copper's exceptional qualities, including its high heat conductivity (400 W/(mK), high electrical conductivity (58 × 106 S/m), ductility, machinability, and significant corrosion resistance, make it a desirable material for use in a variety of engineering applications [3]. The typical industries (Figure 3) in which copper is used are aerospace, electronics, automotive, and power generation. Copper and copper alloys are employed in under-water systems due to their high corrosion resistance[2]. Heat exchangers, radiators, electrical connectors, impulse devices (propulsion devices), and other parts needed in the aforementioned areas are all made from copper (Cu).

## 1.4 WAAM Of Pure Copper:

Intricate shape and geometry are needed to suit the demands of copper components such as heat exchangers, radiators, electronic connectors, and impulse devices[4]. Casting, welding, and machining processes are common fabrication methods for copper components. However, there is still no processing method available to create CU components with intricate shapes. The method that potentially overcome these issues is additive manufacturing, sometimes known as 3D printing[4].

Wire or powder are the two types of starting materials that are employed in AM. Because of copper's usual characteristics, fabricating cu powder using AM methods is challenging. Since copper has a very high reflectivity, it reflects around 97 to 98% of the incident laser light, which results in a minimal degree of absorption[5]. This is contrary to the normal AM processes that use powder, such as selective laser melting (SLM), selective laser sintering (SLS), which require laser power source to heat the material. As a result, more laser power is needed to complete the process in order to make up for the loss of laser power caused by reflection[6]. The optical parts are further harmed by the reflected laser light. Copper's greater conductivity causes issues with powder bed solidification.

The Layer-by-layer manufacturing WAAM technique is attracting a lot of interest due to its benefits of high material utilization, cheap cost, and capacity to create complicated geometry. Layer-by-layer deposition is a feature that saves material and shortens the processing time. External tooling, such as molds, fixtures, dies, and other complicated process requirements used in traditional production methods, are not necessary[1]. Since the price of powder is often two to three times that of the wire version of the same material, WAAM is also cost-effective. So WAAM is chosen as the method for producing copper components.

## 1.5 Substrate Preheating:

Due to copper's high thermal conductivity and the WAAM's frequent occurrence of an unfavorable temperature differential, long columnar grains typically develop in some favored orientations in the direction of heat extraction. Due to the columnar grain formation, the mechanical characteristics of the deposited components are anisotropic, rendering them unsuitable for demanding engineering applications[2]. The microstructure of the deposit should be optimized to create randomly oriented equi-axed grains in order to increase the commercial viability of WAAM to produce large-sized components in copper alloys.

However, a reduced thermal gradient during the deposition improves the growth of equiaxed grains by properly preheating the base plate. Preheating the plate also reduces the thermal gradient for the newly deposited layer, leading to less residual stress being created in the finished component[2]. In the present study, pure copper was deposited on the substrate preheated to 300℃.

## 1.6 Numerical simulation of WAAM process:

The complex thermo-mechanical phenomena of additive manufacturing are influenced by several process variables, including as scanning speed, dwell time, feed rate, voltage, current, and materials. Each component, material, and AM process variation requires a different approach to trial and error when producing and certifying additive manufacturing (AM) parts. To enhance the design of AM components, effective and reliable numerical tools that can accurately represent the AM process are required[7].

Building numerical models that can accurately predict defect development or solidification structure under any given process parameter is therefore crucial for additive manufacturing (AM) technologies. Instead of using experimental approaches, numerical simulations can accurately represent the melting pool, which is required for predicting residual stresses, distortions, and grain structure and texture.

Multi-pass welding and the WAAM strategy are quite similar from a modelling standpoint[7]. The molten pool, which demonstrates intricate physical processes, controls the transfer of heat and mass between the arc and the workpiece. Despite several studies focusing on molten pool and arc dynamics simulation, the relatively high computational time requirements prevent the adoption of such complicated techniques at the component scale level. As a result, coupled thermo-mechanical Finite-Element (FE) studies are frequently used to simulate the process. In essence, a heat source that defines a heat generation per unit volume in the molten pool region is used to describe the heat transfer from the arc to the molten pool. Certain elements activation techniques are used to account for material deposition (element activation technique in the present case).

# Chapter 2: LITERATURE REVIEW

Colopi et al. [6] discusses the challenges and solutions in using selective laser melting (SLM) to process pure copper powders. The high reflectivity and thermal conductivity of copper make it difficult to obtain pore-free products, but the use of high-power fiber lasers and multi-pass scanning strategies can improve part density. The study investigates the effect of different base plate materials and multi-pass scan strategies on the apparent density and productivity of the process. The results indicate that an AISI 316L base plate is more suitable for a stable SLM process of pure copper powder, while the use of a C110 mask compared to the C110 base plate slightly improves the densification behavior. The paper concludes that careful adjustment of process parameters is necessary for SLM processing of pure copper, and high power-high scan speed combinations with a base plate with lower conductivity are advantageous for maintaining a stable process.

Ikeshoji et al.[5] investigated the selective laser melting (SLM) of 99.9% pure copper powder using a high laser power of 800 W. The study builds cube specimens with varying hatch pitch and finds that the highest relative density of 96.6% is obtained at a hatch pitch of 0.10 mm. Transient heat analysis is conducted to estimate the dimensions of the melt pool during the SLM process, revealing instability for narrower hatch pitch and slight overlap for wider hatch pitch. The results suggest that the high conductivity of copper can cause lack-of-fusion voids for both narrower and wider hatch pitch. The study concludes that the findings can be useful for optimizing the SLM process for copper and other high-conductivity materials.

Guschlbauer et al. [4] did a study on the use of selective electron beam melting (SEBM) to produce pure copper parts. The study examines the powder feedstock, process window, microstructure, electrical and thermal conductivity, and mechanical properties of the SEBM-produced copper parts. The results showed that SEBM can produce copper parts with high purity, good density, and acceptable mechanical properties. However, crack formation is a potential issue, and the role of copper oxide at grain boundaries on degrading mechanical properties requires further investigation. The study focuses on the development of a process window for manufacturing dense and crack-free components using pure copper SEBM specimens.

S. Yadav et al. [3] performed a study on the use of Laser Directed Energy Deposition (LDED) for additive manufacturing of bulk copper structures and the characterization of their microstructure and mechanical properties. The study identifies the process window for depositing pure copper on SS 304 L substrate by LDED and evaluates the porosity of the deposit. The increasing LEPF scheme in the range of 9-22.5 kJ/g LEPF between two subsequent layers yielded bulk deposits without interlayer and interlayer porosity, with relative density around 99.9%. The study concludes that LDED can be used to deposit pure copper bulk with fine grain structure and high mechanical strength, and highlights the potential of LDED for fabricating copper components for various engineering applications.

Yingang Liu et al. [8] explored the use of laser powder bed fusion (L-PBF) additive manufacturing to fabricate high-strength copper alloys with a heterogeneous grain structure through the inoculation of pure copper powder with cobalt submicron particles. The study investigates the microstructure and properties of the Cu-Co alloys, including XRD diffraction spectra, grain morphology, and crystallographic orientation. The addition of Co was found to refine the grain size and modify the grain morphology, resulting in a heterogeneous grain structure. The study also identified the presence of CoO nanoparticles in the microstructure, which were formed during solidification of the melt pools. The findings provide insights into the development of high-performance copper-cobalt alloys for various applications. The paper also discusses the use of selective laser melting (SLM) to manufacture copper alloys with improved mechanical properties.

Yadav et al. [9] reports on an experimental investigation of the laser additive manufacturing (LAM) of copper tracks on stainless steel 304L using a LAM-directed energy deposition (DED) system. The study aimed to understand the effect of process parameters on LAM-DED for fabricating bimetallic joints and graded structures of copper and SS304L. The study finds that the track geometry is significantly affected by the combined effect of process parameters, and continuous and defect-free deposition is observed between 6 and 18 kJ/g LEPF. The major reason for variation in track geometry with an increase in scan speed is due to the reduction in laser energy available and interaction time. The study also finds that the deposition rate is mainly governed by laser power, followed by powder feed rate and scan speed. The study concludes that the findings can aid in the fabrication of bulk samples and bimetallic joints or functional graded joints of Cu and SS304L.

Dong et al. [10] discusses the use of wire arc additive manufacturing (WAAM) process to produce copper-aluminum (Cu-Al) alloy with a desired chemical composition and full density. The study found that the WAAM process can produce a homogeneous alloy with a desired composition and hardness after homogenization annealing. The microstructure, phase characterization, composition, and hardness of the fabricated alloy are analyzed. The results show that the Al content and hardness are non-uniform in the dilution-affected zone due to the slower feed speed of pure Al wire and the high thermal conductivity of the copper substrate. However, the chemical composition and hardness become more homogeneous after a few layers above the dilution-affected zone. The article concludes that further post-fabrication processes, such as cold works and more advanced annealing processes, will be carried out to improve the material and mechanical properties of additive manufactured Cu-Al alloys.

Baby et al. [2] discusses the development of equi-axed grain structures in copper-based components produced through wire arc additive manufacturing (WAAM). The study focuses on optimizing metal transfer characteristics in a gas metal arc-based WAAM process to generate isotropic microstructures. The results show that short-circuiting metal transfer produces equi-axed and fine-grained microstructures with isotropic mechanical properties. The paper also discusses the various techniques used to achieve equi-axed grain structures during WAAM and their limitations.

Desmukh et al. [11] investigated the feasibility of using Wire Arc Additive Manufacturing (WAAM) to fabricate pure copper wall structures. The study found that the WAAM-built pure copper exhibited high tensile strength and ductility, with an enhanced percentage elongation. The study concludes that WAAM can be used to fabricate fully dense and defect-free pure copper with desired optimum mechanical properties.

EL-Wardany et al. [12] discusses the challenges associated with additive manufacturing of copper coils for ultra-high efficiency induction motors used in aerospace and electric vehicle applications. The paper proposes different approaches to overcome these challenges, including copper powder treatment, physics-based modeling of the laser powder deposition process, and the use of alternative copper alloys. The article also discusses the development of a simulation tool called SAMP for laser powder bed and laser powder deposition processes. The results show that these approaches can reduce porosity and improve density, but impurities in the starting powder can still affect electrical conductivity. Further research is needed to optimize the process parameters and control impurities for better conductivity.

Williams et al. [13] explored the use of wire and arc additive manufacturing (WAAM) for depositing pure copper, which has high thermal and electrical conductivity. The study found that WAAM can successfully deposit pure copper with very high electrical conductivity (102%) under optimized conditions. However, a fully shielded environment is needed to avoid porosity and achieve high conductivity levels. The article also discusses the use of copper alloys in additive manufacturing and provides information on their properties and conductivity. The study concludes that WAAM can be a viable option for depositing pure copper with high conductivity, but proper shielding and optimization are necessary.

Goldak et al. [14] presents a new mathematical model for welding heat sources based on a Gaussian distribution of power density in space. The model proposes a double ellipsoidal geometry that can easily change the size and shape of the heat source to model both shallow and deep penetration welding processes. The model is compared to previous models and experimental results, showing excellent agreement. The article emphasizes the importance of accurate modeling of the weld heat source in predicting residual stress, distortion, and strength of welded structures. In conclusion, the double ellipsoidal model is found to be more accurate than conventional analytical solutions and can be adapted to different welding geometries. The article provides technical details and equations for the model and includes verification of the model through analysis of two different welding situations. The paper highlights the significance of accurate modeling of the weld heat source in predicting the behavior of welded structures.

Singh et al. [15] paper reviews the use of modeling and simulation in additive manufacturing processes, with a focus on addressing the challenges of AM such as mechanical and chemical properties, microstructure, and dimensional stability. The article also discusses the use of multi-scale modeling and simulation techniques in polymer nanocomposites and the different categories of computer simulation. The goal of AM modeling is to predict the functional and load-bearing capacity of end products and control their properties and design. The simulations are used to determine dynamic and static properties of PNCs, such as thermal and electrical conductivity, bulk modulus, and diffusion coefficient. The article concludes that computer simulation methods are essential for studying the structure and properties of PNCs and for predicting the functional and load-bearing capacity of end products in additive manufacturing.

Geng et al. [16] presented a multi-scale modeling approach to investigate the microstructure, micro-segregation, and local mechanical properties of Al-Cu alloys in wire and arc additive manufacturing (WAAM). The study focuses on the influence of process parameters, such as welding current and substrate moving speed, on temperature distribution, microstructure evolution, and micro-segregation. The results show that substrate moving speed had a significant impact on dendrite morphology and size, while increasing the current generated larger temperature gradients. Micro-segregation was observed between dendrites or even cracks in the solidified microstructure due to the fast-cooling rate in WAAM. The study used a multi-scale model combining the phase field and finite element methods to investigate the microstructure evolution and element distribution in the wire arc additive manufacturing (WAAM) solidification process. The simulated results were validated through metallographic examinations, EDS tests, and miniature tensile tests. The study concludes that the UTS and elongation could be improved simultaneously by increasing the moving speed of the substrate, while an increased current resulted in a deterioration of the mechanical properties.

Feng et al. discusses the numerical simulation of residual stress and deformation in wire arc additive manufacturing. The study includes multi-layer and multi-pass arc additive manufacturing experiments on Q345 substrate using Y309L welding wire. The effects of substrate thickness and interpass temperature on temperature field, stress field, and deformation were discussed. The simulation consisted of two parts: thermal analysis and mechanical analysis. The results showed that a low interpass temperature and thin substrate were able to effectively reduce the tensile residual stress. The thick substrate resulted in a small angular deformation of the substrate during the additive manufacturing process. Increasing substrate thickness can reduce interpass temperature and tensile residual stress, but also increase the risk of brittle fractures. The finite element method developed is reliable for predicting angular deformation of the substrate. The article concludes that the research provides valuable insights into the effects of substrate thickness and interpass temperature on the thermal cycle, residual stress distribution, and deformation evolution during additive manufacturing. The findings can be used to optimize the process parameters and improve the quality of additively manufactured materials.

Ning An et al. [17] presents the implementation and verification of finite element simulation techniques for thermal analysis of electron beam melting (EBM) additive manufacturing process. The authors developed Abaqus user subroutines and a plugin tool called AM Modeler to simulate the heat transfer phenomena in the EBM process. The accuracy of the simulation techniques was verified and validated through comparison with numerical and experimental results. The simulation results demonstrate the capability of the proposed simulation techniques. The study contributes to the enhancement of understanding of the EBM process and provides helpful case studies and available source codes for users either from academia or industry. In conclusion, the proposed simulation techniques can be used to optimize the EBM process and improve the quality of the printed parts.

Bonifaz et al. [18] discusses the development of a mechanical model for the wire + arc additive manufacturing process. The model aims to predict material properties by linking processing variables to resulting plastic strains and residual stresses. The study found that thermal stresses increase with the increase of weld speed or the heat distribution parameter, while local plastic strains increase with the increase of welding speed but not necessarily with the heat distribution parameter. The level of thermal stresses and local plastic strains is lower in each new successive AM layer due to the relief of thermal stresses and plastic strains by preheating. The study establishes a firm foundation for thermo-mechanical modeling in the WAAM process. In conclusion, the paper provides valuable insights into the WAAM process and its potential for predicting material properties.

F_montevecchi et al. [7] proposed a new finite element modeling strategy for the Wire-Arc-Additive-Manufacturing (WAAM) process, which takes considers the actual power distribution between filler and base materials. The proposed model includes a novel heat source model and an element activation strategy, as well as an alternative way to include latent heat of fusion effects without causing convergence issues. The proposed process modeling was validated and compared with traditional heat source modeling, and was found to achieve higher accuracy without the need for time-consuming tuning operations. An experimental validation is provided by comparing the measured distortions of a WAAM test case with the simulated ones, highlighting the accuracy of the proposed model. In conclusion, the proposed finite element modeling strategy for WAAM process improves accuracy and simplifies model parameter set up. The model takes into account the actual power distribution between filler and base materials, which is a significant improvement over traditional heat source modeling. The experimental validation shows that the proposed model achieves higher accuracy without the need for time-consuming tuning operations. This paper contributes to the development of more accurate and efficient modeling techniques for wire and arc additive manufacturing processes.

Tangestani et al. [19] created a computational WAAM model that may be utilized to forecast the residual stresses resulting from, without conducting the experiment, to rolling. The stainless steel (SS) material used in the WAAM model is placed on a structural steel substrate, and the layers are formed as the heat source moves along the designated path. The thermo-mechanical properties that can be obtained from this computational model can be used for analysis to forecast the residual stress of the end component. The experiment is next run using the same materials and parameters to validate these numerical results. Since the validation results are essentially the same, this research approach can be applied without doing any experiments.

# Chapter 3: MOTIVATION, OBJECTIVES AND RESEARCH METHODOLOGY

## 3.1 Motivation

Casting, welding, and machining processes are common fabrication methods for copper components. However, as Cu is used to make a variety of components, including heat exchangers, radiators, and electrical connectors, complicated and sophisticated shapes are needed that are difficult to create using the above-mentioned standard processes[4]. A processing method to create Cu components with complex forms is still lacking. The approach that could fix these issues is WAAM. In order to reduce residual stress induction, the current study focuses on fabricating copper components using the WAAM technology and substrate preheating. To the best of the author's knowledge, there is no literature on WAAM processing of copper with substrate preheating and very limited literature regarding WAAM processing of copper. Additionally, because there are so many factors involved in WAAM processing, optimization is a crucial and time-consuming experimental job, necessitating the necessity for an appropriate numerical simulation of the procedure. As a result, the process' numerical simulation is also carried out.

## 3.2Objectives

- Fabrication of copper wall structure at optimized parameters with and without substrate preheating
- Investigation of mechanical and microstructural characterization of deposited copper wall structure.
- Comparative study of mechanical properties of copper bulk fabricated through with and without substrate preheating.
- Development of a Numerical simulation model of WAAM process
- Validation of the results obtained from numerical simulation.

## 3.3 Methodology of Research

- Literature survey of previous works
- Identification of Objectives of thr project
- Experimental iterations to optimize parameters
- Deposition of Cu Wall with and without substrate preheating
- Mechanical and microstructural characterization
- Comparative study of properties of different depositions
- Numerical simulation of WAAM process
- Validation of simulation with experimental results
- Results discussions and conclusions
- Future scope

To the best of the author's knowledge, there is a lack of sufficient literature regarding the WAAM processing of pure copper, and there is no available literature addressing the impact of substrate preheating on the microstructure and mechanical properties of pure copper. The presented work involves the experimental deposition of pure copper wall structure on a mild steel substrate. The process parameters were optimized, and the deposition was performed with and without preheating the substrate. The deposited wall structure was cut, and samples were extracted along the building and scanning directions using a Wire Electric Discharge Machine. The extracted samples were then prepared for microstructure studies using standard metallographic techniques and observed under an optical microscope (Leica DMS 1000). Microhardness testing was conducted using a Vicker's microhardness tester (Omnitech, MVH-S Auto) with a 30g load and a 10-second dwell period. Micro tensile testing was performed using a Universal Testing Machine (Instron, model: 5982) with a strain rate of 1mm/s and a maximum load capacity of 10 kN. Fractography of the tensile samples was analyzed using a scanning electron microscope (SEM). Scratch tests were conducted at a speed of 0.2 mm/s, with loads of 5 and 10 N, and a scratch length of 2mm. X-Ray diffraction (XRD) analysis was performed on the samples and residual stresses were obtained along building direction.

Once the experimental phase was completed, the WAAM process was modeled numerically using Abaqus 6.13 software, along with Python and Fortran codes. Temperature profiles were predicted and utilized as input for the mechanical model, which was developed to estimate residual stresses. The preheating temperature was varied, ranging from room temperature to 100°C, 200°C, and up to 600°C. The generated residual stresses from the model were subsequently compared to the Residual data obtained from literature[20], and validated.

# CHAPTER 4: WAAM OF PURE COPPER

## 4.1 Experimental Setup:

The Schematic of experimental setup as shown in Figure 4 mainly consists of Electric arc power source, CNC system, wire feeder, computer system, and argon gas cylinder. DC electric arc power source is used to produce arc between the workpiece and substrate. In GMAW based WAAM feedstock wire itself acts as the positive electrode so that maximum heat is produced in the wire end for it to get melted quickly.

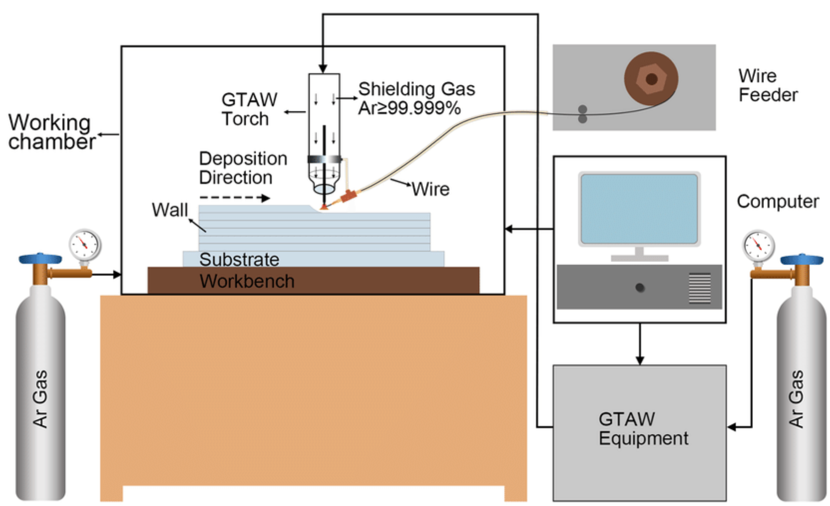


Figure 4 Schematic of GMAW based WAAM system [26]

CNC system is used to move the welding torch in all three axes. The motion of CNC system is controlled through a software in computer system (“MACH3” in present case). G & M codes are provided to guide the motion along different axes. Torch travel speed is also specified in the code. The role of wire feeder it to continuously supply wire to the system. Wire feed rate can be controlled with the help of a knob present in the wire feeder itself. Since during the processing the system is exposed to high temperatures, to prevent oxidation and atmospheric contaminants of the final component, argon or inert gas is used. The supply or the flow rate of the gas is also controlled through the knob.

## 4.2 Substrate Preparation:

According to Colopi et al.[6], the base plate's thermal conductivity and type are critical for preserving the process stability and the powder bed temperature. Because of its extremely high heat conductivity, using C110 is challenging. Although influential, cutting the base plate thickness does not effectively reduce heat transfer. Due to the decreased thermal conductivity, using a mild steel or stainless-steel base plate offers thermal stability.

The base plate was cut with the dimension of 100*100*100 mm with the help of a plasma arc cutting machine. The sides of the plate were made straight with the help of a belt grinder. The plate was further cleaned with acetone before depositing over it.

## 4.3 Process Parameter Optimization:

Wire arc additive manufacturing (WAAM) typically involves a large number of parameters to control for smooth deposition. The typical process parameters are wire feed speed (m/min), torch travel speed (mm/s), voltage, current, inert gas flow rate etc. To achieve smooth, continuous and defect free deposition, all these parameters are needed to be controlled.

Initially, pilot experiments were conducted to optimize the process parameters. Multiple single and multi-layer tracks were deposited as shown in Figure 5 by varying the parameters.

Figure 5 Experimental Iterations to optimize parameters

The single tracks which showed most smooth deposition with minimum defects and spatter were further checked for multi-layer bonding. The parameters which yielded for smooth single track and good inter-layer bonding were then selected as the final parameters for bulk copper wall deposition.

## 4.4 Fabrication of copper wall structure

Figure 6 Deposited Cu wall structure on non-preheated sample

Figure 7 Deposited Cu wall structure on preheated sample at 300℃

After the completion of process parameter optimization, copper wall bulk structures were deposited on the mild steel base plate. Figure 6 and Figure 7 shows the final deposited structures. The final optimized parameters are shown in the Table1 below.

Table 1 Optimized process parameter for Cu bulk deposition

| **Parameters** | **Non-Preheated sample** | **Preheated sample (300℃)** |
|---|---|---|
| Base plate material | Mild steel | Mild steel |
| Base plate dimension | 150*150*10 mm3 | 150*150*10 mm3 |
| Work Material | Pure copper wire | Pure copper wire |
| Wire dia | 1.2 mm | 1.2 mm |
| Voltage | 15.5 V | 13.8 V |
| Wire feed rate | 5 m/min | 3.9 m/min |
| Scan speed | 500 mm/min | 300 mm/min |
| Argon flow rate | 20 l/min | 25 l/min |

# Chapter 5: NUMERICAL SIMULATION OF WAAM PROCESS

## 5.1 Methodology and flow chart:

Abaqus 6.13 software is used to carry out the numerical simulation of the WAAM process. To simulate the entire deposition process, a finite element study is conducted, which models the movement of a heat source and the addition of layers. Figure 9 shows the flow chart of the simulation process. Two types of finite element analysis are performed to predict the final parameters of the WAAM process. The first is a thermal analysis, which obtains parameters such as heat flux distribution and temperature distribution that serve as input for the mechanical analysis. The mechanical analysis then provides parameters such as Von Mises stress, principal stress, and residual stress of the component.

The simulation of WAAM process mainly involves the simulation of heat transfer from the arc to the material and layer-by-layer deposition. The heat transfer from arc is simulated by the Goldak double ellipsoidal heat source model. The parameters of the model are defined in the DFlux subroutine, written in Fortran language. The layer-by-layer deposition was then performed by the introduction of a python script to automate the process.

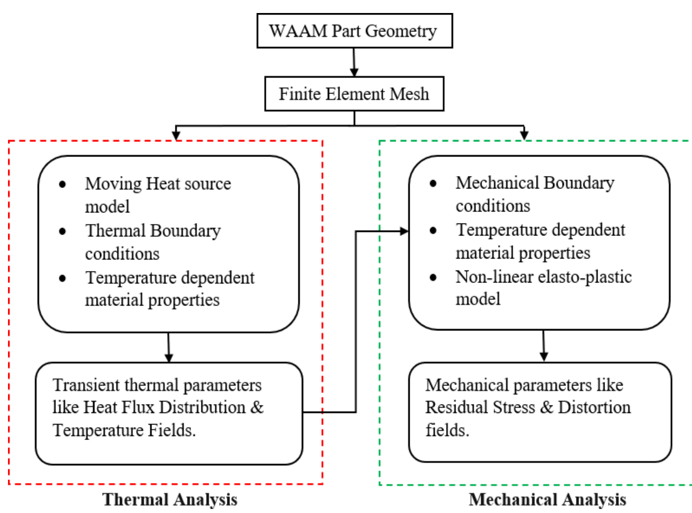


Figure 8 Flow chart of numerical simulation

## 5.2 Goldak heat source model:

The Goldak heat source model[14] is employed in the majority of research dealing with AM modelling[7]. A moving double ellipsoid region receives the heat input in this model using Gaussian distribution.

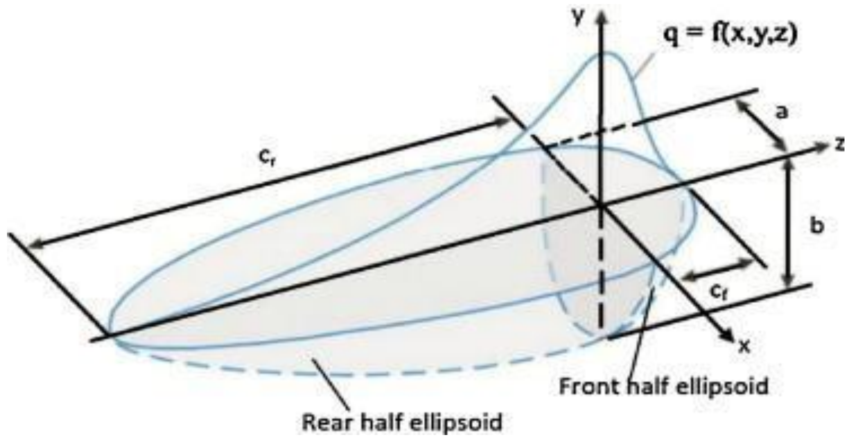


Figure 9 Goldak Double Ellipsoid Heat source

The coefficients a, b, and c_f and c_r are shown in Figure 10 as the semi-axes of two ellipses that are centered on the frame of reference's origin. Due to the double subscript of the argument a, two separate functions are generated using different values (c_f if positive and c_r if negative). An ellipsoid surface is used to depict the region of space where the power density is reduced to 5% of its maximum value. The semi-axes of the ellipsoids are typically valued according to the size of the molten pool [15]. The frontward and backward ellipsoids have different values for the distribution factors, abbreviated as f_f and f_r, respectively.

The DFLUX subroutine is used to define the ellipsoidal parameters and the heat source equations with respect to time, in order to represent this GOLDAK heat source. When the heat source model passes over the base plate, the elements of the wall that were initially deactivated become sequentially active.

### *5.2.1 Boundary conditions and Heat source equations*:

$$Q\,(x, y, z, t) = \begin{cases} Qf \text{ for } z \geq z0 \\ Q_r \text{ for } z \leq z0 \end{cases}$$

$$Q_f\,(x, y, z, t) = \frac{6*\sqrt{3}*Q*f\_f}{a*b*c*\pi*\sqrt{\pi}} * e^{-3\{(\frac{x}{a})^2+(\frac{y}{b})^2+(\frac{z}{c\_f})^2}$$

$$Q_r\,(x, y, z, t) = \frac{6*\sqrt{3}*Q*f\_r}{a*b*c*\pi*\sqrt{\pi}} * e^{-3\{(\frac{x}{a})^2+(\frac{y}{b})^2+(\frac{z}{c\_r})^2} \qquad [14]$$

Where $\varepsilon$ = z + $\nu$*$(\tau - t)$ and a, b, c_f, c_r are ellipsoidal parameters.

Q = Heat input = η*I*V (in Watts)

$Q_f$ = Front ellipsoid heat flux

$Q_r$ = Rear ellipsoid heat flux

$$\frac{f\_f}{c\_f} = \frac{f\_r}{c\_r}$$

Where f_f +f_r = 2

### *5.2.2 Parameters used for simulation*

| Symbol | Parameter | Preheated samples | Non-Preheated sample |
|---|---|---|---|
| Q | Heat Input | 1000W | 1600W |
| V | Scanning speed | 5 mm/s | 8.33 mm/s |
| F | Feed rate | 3.9 m/min | 5 m/min |
| f_f | Heat fraction coefficient in front ellipsoid | 0.6 | 0.6 |
| f_r | Heat fraction coefficient in rear ellipsoid | 1.4 | 1.4 |
| $c_f$ | Length of the front ellipsoid | 1 mm | 2 mm |
| $c_r$ | Length of the rear ellipsoid | 4 mm | 6 mm |
| a | Width of the ellipsoid | 3 mm | 3mm |
| b | Depth of the ellipsoid | 3 mm | 3mm |

The ellipsoidal parameters are selected based on the experimental data obtained. The parameter 'a' is selected based on the bead width, 'b' was calculated based on the bead height, 'c_f' and 'c_r' were selected based on the scan speed, as to how much length of the material is deposited in single step of simulation.

## 5.3 Abaqus Analysis procedure

Each module in ABAQUS/CAE defines a logical step in the modelling process, such as establishing the geometry, specifying the properties of the materials, and creating a mesh [20]. Each module is used for specific purpose and then the complete model is developed. The model is then submitted in ABAQUS/CAE then generates an input file that is send to the ABAQUS analysis product after the model is finished. The input file created by ABAQUS/CAE is read by ABAQUS/Standard or ABAQUS/Explicit, which then does the analysis, provides data to ABAQUS/CAE so that job's progress can be tracked, and creates an output database. In order to visualize the outcomes of the analysis, the output database is read using the Visualization module.

The present analysis makes use of 9 modules out of 11 modules as shown in the Figure 11. All those nine modules are described below.

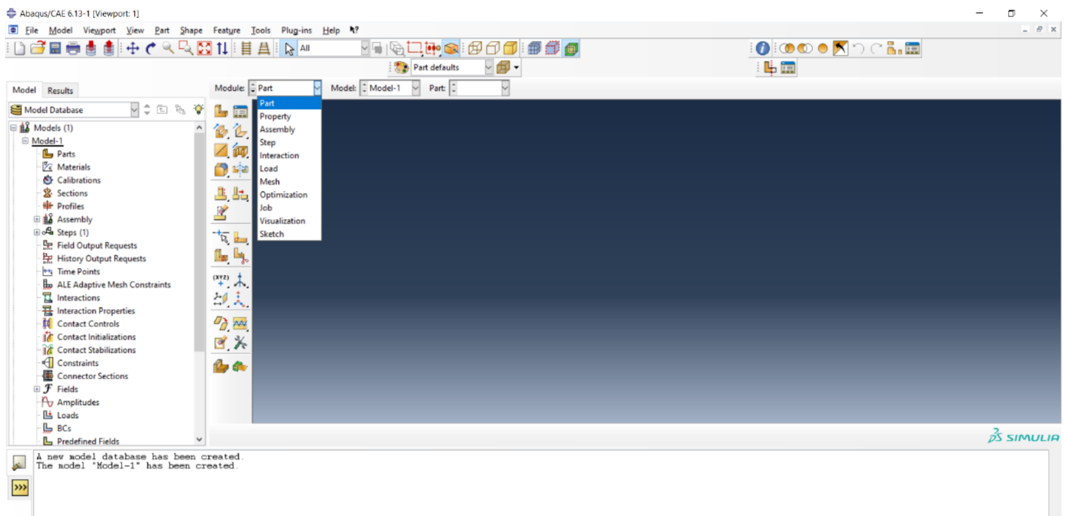


Figure 10 Abaqus GUI

**Part Module:** This module is used to define the geometry of deposition. The base plate was of dimension 100*100*10 mm and Cu wall was extruded over the plate with the dimension of 100*6*30 mm (since each layer was of height 3mm and there were 10 layers, so the total height came to be 30 mm).

**Property Module:** This module is used to define the temperature dependent material properties to be used during analysis. Two different sections (base plate section and Cu wall section) were made to assign different properties to different parts of the model.

**Assembly Module:** In Abaqus, a model typically has one primary assembly that is made up of actual instances of model pieces. As a result, the part that was created in the part module was created as an instance in this module.

**Step Module:** Analysis in Abaqus usually consists of various types of steps defined. For the present analysis we defined a heat transfer step for thermal analysis and static-general step for mechanical analysis. The deposition of each layer was divided into 20 steps, each of 1 second time period. A wait step was also defined at the start of the step module, which is used to deactivate all the elements in the interaction step at the start of the process. So, there were a total of 202 steps (initial, wait and 200 welding steps). The 'initial' step is by default step created in the Abaqus, which cannot be deleted or modified.

**Interaction Module:** This module is a step dependent module, that means different interactions are defined for different steps. Multiple interactions can also be created for a single step. There are different types of interactions available for different types of analysis steps (heat transfer or static-general step etc). The 'Model Change' interaction is used to activate and deactivate the elements at various steps. It was first created at 'wait' step to deactivate all the Cu wall elements at the start of the analysis. Sequentially, all wall elements were then activated at suitable time step using the same interaction. Radiation and convection interactions were also introduced at 'wait' step during thermal analysis which was then propagated to all other steps.

**Load Module:** This module is used to define the load at various steps. This module is also step-dependent. There are different types of loads for different types of steps (heat transfer or static-general step etc). In the present analysis 'Body Heat Flux' was used in the thermal analysis. The Load was of 'User-defined' (since Goldak heat source model has user defined parameters) type and was included in the model using Fortran written DFlux subroutine. The subroutine is attached to the job file before the analysis starts.

During thermal analysis, the preheating of the base plate is done by defining PreDefined Field of suitable temperature value. In the mechanical analysis there was no external load applied. However, the thermal field generated during the thermal analysis is introduced as the 'PreDefined Field' which is also present in the load module. Boundary conditions are also defined using this module.

**Mesh Module:** This module is used to create the mesh on the assembly or part created. Different mesh sized for different areas were used for the analysis to reduce computational time. The mesh size was kept 3 and 5 mm for the present analysis. Also, the element type is defined in this module. For Thermal analysis it was defined as “Heat Transfer” elements and for mechanical analysis it was defined as “3D stress” element.

**Job Module:** After all the analysis steps and previously defined modules are completed, the job module is used to submit the job, along with attaching the DFlux subroutine. The progress of the job and any error or warning can be seen in the window displayed on the job module.

**Visualization Module:** Finite element models and results are graphically displayed through the Visualization module. It pulls model and result data from the output database; by adjusting output requests in the Step module, one can manage what data is stored there. This module is used to see the various results of the completed job. A two-dimensional graph of one variable in comparison to another called an X-Y plot can also be plotted.

## 5.4 Thermo-Mechanical analysis

The thermal analysis was first carried out using all the Abaqus modules that had been previously defined. The heat input was simulated using the previously explained Goldak heat source model defined using Fortran written Dflux subroutine and the layer-by-layer deposition of the material is carried out using deactivating and activating interactions. The steps, interactions and loads for this layer-by-layer deposition were created using the python scripts. The ABAQUS 6.13 program was then merged with this PYTHON script and the DFLUX subroutine to carry out the task analysis. The distribution of temperature and heat flux, among other thermal characteristics, was acquired.

After that, the mechanical analysis used the temperature distribution from the thermal analysis as an input pre-defined field, and mechanical parameters like principal stress, residual stress, etc., were obtained at each increment throughout the entire simulation of the WAAM process. Chapter 6 provides a description of the thermo-mechanical analysis' findings.

# CHAPTER 6: RESULTS AND DISCUSSIONS

## 6.1 Microstructure Studies:

(i)

(ii)

(iii)

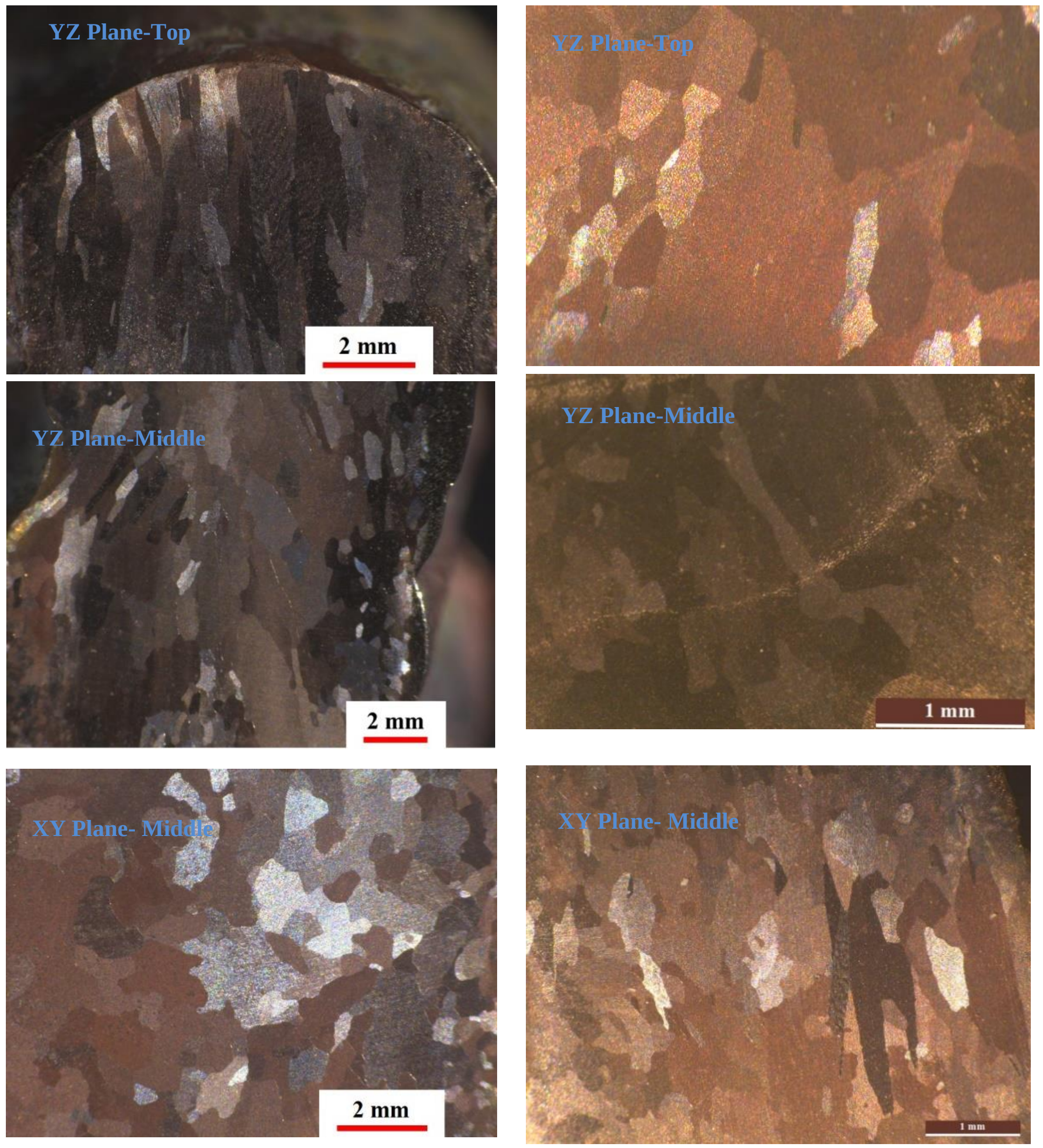


**(a)** **(b)**

Figure 11 Microstructure of Non-Preheated (a) and Preheated samples (b)

The optical microscope (make and model: Leica DMS 1000) is used to conduct the microstructure research. As seen in Figure 11 (a)(iii), the equiaxed grains are seen along the SD for both the samples; however, the grains are finer in the case of preheated samples. This is because the primary direction of heat transfer is along the building direction, and thus the heat extraction does not take place at a high rate in the scanning direction. But considering the microstructure along the building direction from bottom to top for both the non-preheated sample (Figure 9 a (i, ii), cellular grains and refined equiaxed grains can be found in the bottom area. This is explained by the quick heat transfer from the WAAM-deposited high conductivity Cu to the substrate due to a high-temperature gradient [11]. In the center section, equiaxed grains become columnar, and in the top region, fully grown columnar grains are visible. As a result, the deposit's build direction coincides with the realization of the epitaxially developed grain structure. The directional solidification phenomenon is thought to be responsible for the development of epitaxial grain structure along the build direction from bottom to top [11]. According to it, grain growth in the bulk weld deposit is significantly easier in the direction parallel to the rising temperature gradient.

Considering the microstructure of the preheated sample, In the building direction, there is columnar grain growth, but the grains are coarser compared to non-preheated sample due to substrate preheating and heat accumulation effect. Also, the top portion shows more equiaxed grain formation due to direct exposure to atmosphere and preheating effect.

## 6.2 Hardness Measurement

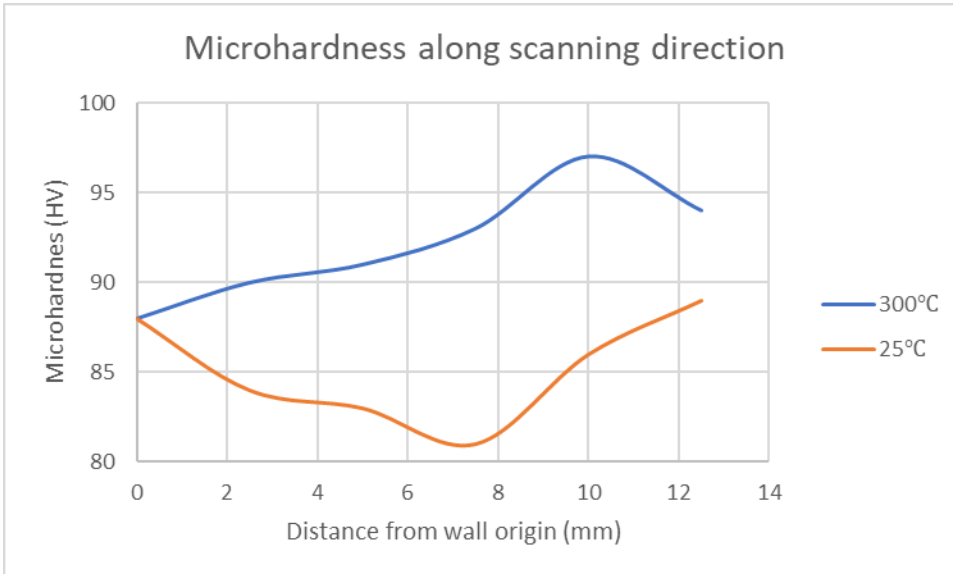


Figure 12 Micro Hardness along scanning direction

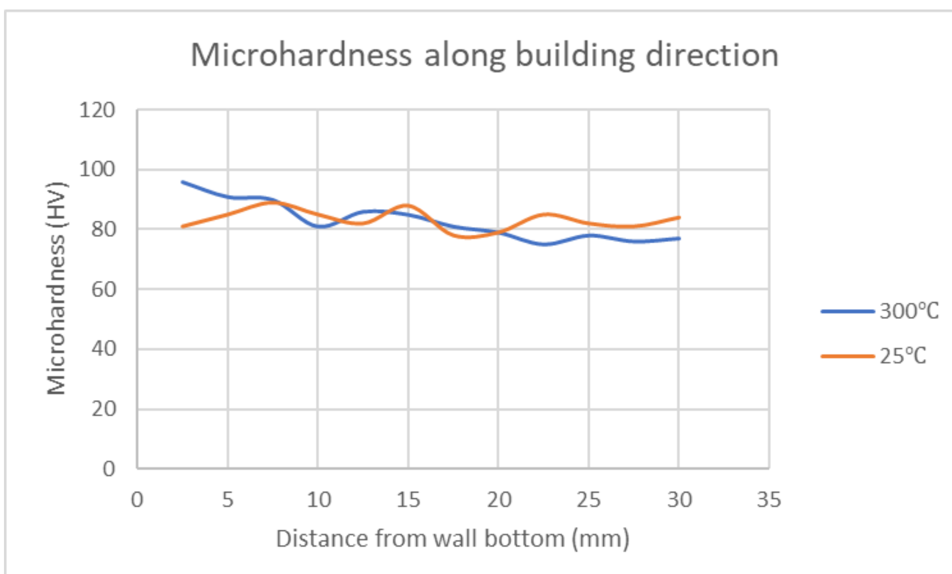


Figure 13 Micro Hardness along building direction

The Vickers microhardness test was conducted using the Omnitech MVH-S Auto microhardness tester. A load of 30g and a dwell period of 10 seconds were applied. In the scanning and building directions, the non-preheated sample exhibited an average microhardness value of 85 HV and 83 HV, respectively. The microhardness value did not vary significantly in the scanning direction due to the presence of a uniform microstructure throughout. However, along the building direction, there was more variation in the value attributed to epitaxial grain growth. As for the preheated sample, its average microhardness values along the scanning and building directions were 92 HV and 81 HV respectively.

As the grains becomes finer, more grain boundaries are formed, which hinders dislocation movement and increases the hardness of the material[3]. The pre-heated base plate reduces the thermal gradient between the wall and substrate surface, so more refined grains are formed, which has led to slightly increased hardness value of preheated sample along the scanning direction. However, columnar grains are formed along building direction. Thus, the value does not differ for both samples along it.

## 6.3 Tensile Test

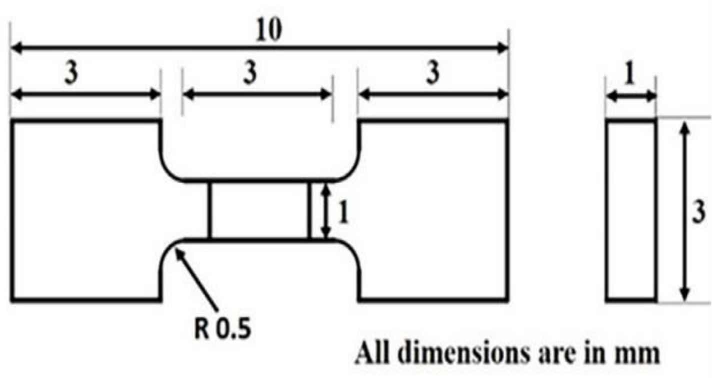


Figure 14 Micro Tensile specimen dimension

Micro tensile testing was performed using a Universal Testing Machine (UTM, make: Instron, and model: 5982) with a strain rate of 1mm/s and having maximum load capacity of 10 kN. The micro tensile samples were cut along scanning direction and building direction with the dimension as shown in the figure.

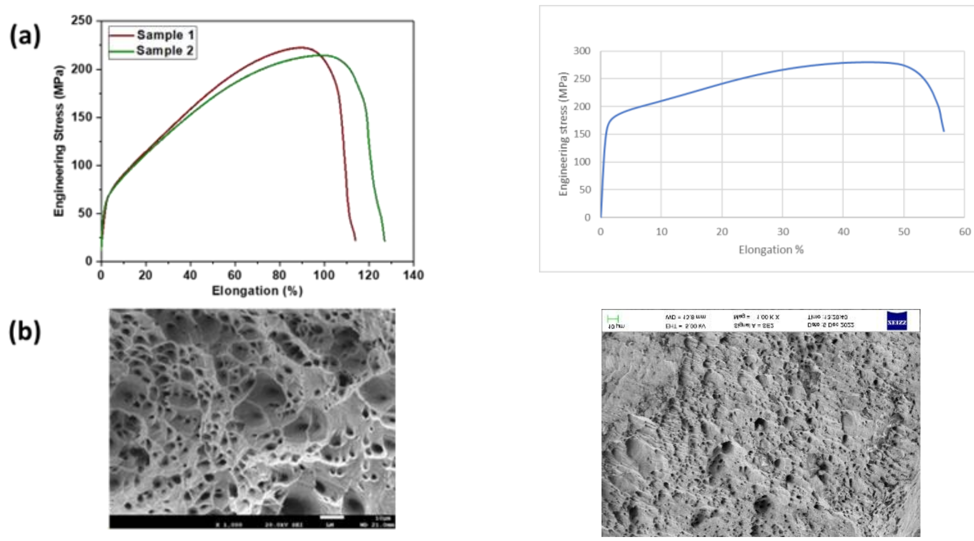


(i) (ii)

Figure 15 Tensile strength curve along scanning direction ((i): non-preheated sample, (ii): preheated-sample)

The UTS along scanning and build direction for preheated and non-preheated samples are 280 MPa, 224 MPa and 225 MPa, 220 MPa respectively. The pre-heated sample shows enhancement in the tensile strength of the material along the scanning direction because of the presence of finer grains. This is because preheating the substrate before the AM process can have positive effects on the tensile strength of the material. By preheating, the thermal gradient between the deposited material and the substrate is reduced. This reduction in thermal gradient helps in minimizing the presence of residual stresses and can promote better metallurgical bonding between the layers [2].

(c)

(d)

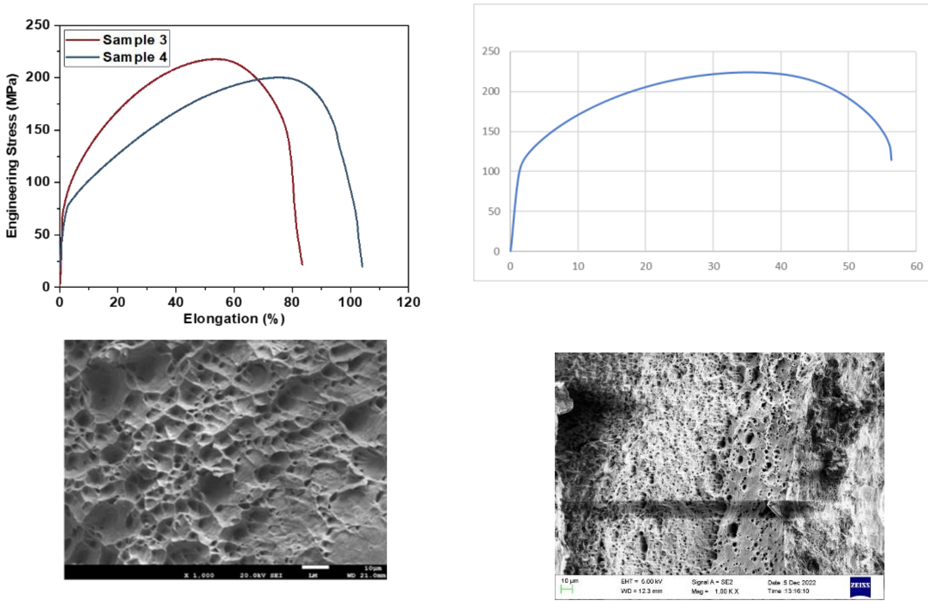


(i)

(ii)

Figure 16 Tensile strength curve along building direction ({i}: non-preheated sample, {ii}: preheated-sample)

At the same time, in the case of a non-preheated sample, higher thermal gradients and increased residual stresses can be expected. These factors can negatively impact the tensile strength of the material. High thermal gradients can lead to uneven cooling rates and potential defects, such as porosity or cracking, which can significantly weaken the material's tensile strength. However, along the building direction, the UTS of both the samples are almost the same because of the presence of columnar grain structure.

However, preheating has a negative effect on the elongation. Preheating the substrate before WAAM can promote grain growth in the material. The elevated temperature encourages larger grain formation, which can lead to reduced ductility and decreased elongation [3]. Coarser grains generally have less grain boundary area for dislocation movement, limiting the material's ability to deform before fracture.

Fractography of the fractured tensile samples were analysed using scanning electron microscope (SEM). Dimples were seen on the fractured surface of both the non-preheated and preheated samples, which are one of the most characteristic features of ductile fractures. They appear as small, round depressions or voids on the fracture surface. Dimples are formed due to the nucleation, growth, and coalescence of voids or micro voids during plastic deformation before fracture[3]. The size, density, and shape of the dimples can provide valuable information about the ductility and toughness of the material.

## 6.4 Measurement of coefficient of friction

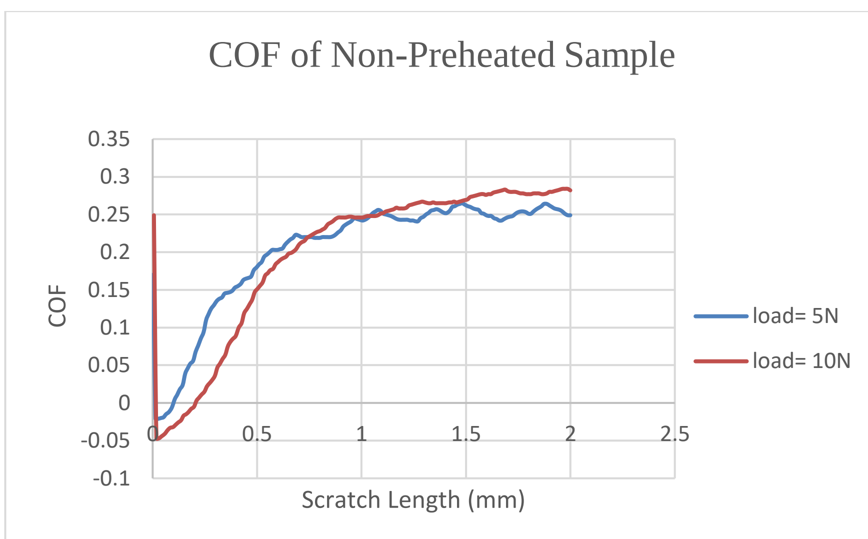


*Figure 17 COF of Non-Preheated Sample*

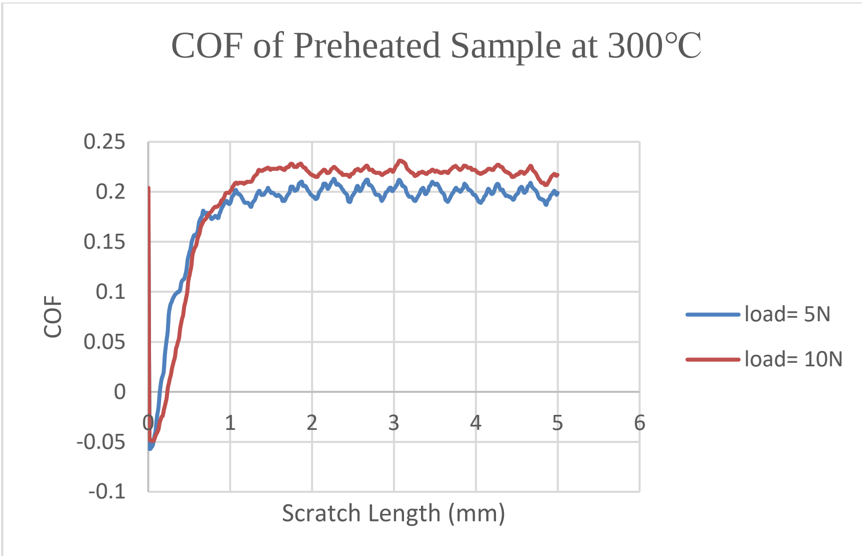


Figure 18 COF of Preheated Sample at 300℃

The scratch test was done at scratch speed of 0.2 mm/s, load of 5 and 10 N and scratch length of 2 mm. The coefficient of friction is a parameter used in tribology to quantify the resistance to sliding or relative motion between two surfaces in contact. It provides information about the frictional behaviour of a material under specific conditions. The coefficient of friction is a dimensionless value that represents the ratio of the frictional force to the normal force acting between the two surfaces. It indicates the level of frictional resistance encountered when one surface slides or rolls against another.

The average COF value at load of 5 N and 10 N for non-preheated sample came about 0.27 and 0.25, whereas for the preheated sample at 300℃ the value is about 0.18 and 0.19 respectively for the corresponding same load. A lower coefficient of friction suggests reduced energy losses due to friction, indicating a more efficient material for minimizing power consumption or improving energy efficiency. Higher coefficients of friction may indicate increased material wear due to higher contact forces and more significant surface interactions. Lower coefficients of friction generally imply improved wear resistance[21]. Hence, it is concluded that preheated sample is better in both frictional efficiency and wear resistance compared to non-preheated sample.

## 6.5 XRD Measurement

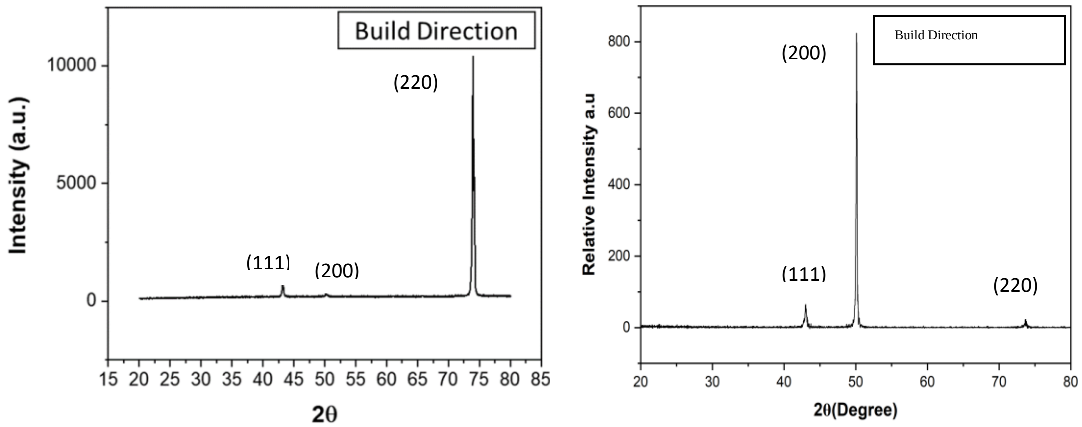


*Figure 19 XRD of non-preheated and Preheated bulk deposited copper structure*

The XRD (X-ray diffraction) graph of pure copper deposition typically exhibits distinctive peaks that correspond to the crystallographic structure of the material. Copper possesses a face-centered cubic (FCC) crystal structure, which gives rise to specific diffraction patterns in the XRD graph. In an XRD graph of pure copper, several strong peaks are observed. The most prominent peak, known as the (111) peak, appears at a diffraction angle (2θ) of approximately 43 degrees. Other major peaks include the (200) peak at around 50 degrees and the (220) peak at around 74 degrees. These peaks represent the preferred orientations of copper crystals in the sample.

The intensities of peaks are slightly different on non-preheated and preheated samples because the exact positions and intensities of the peaks vary slightly depending on the specific experimental conditions and the quality of the copper sample. However, the general pattern of strong peaks corresponding to the FCC crystal structure of copper is consistent in both the XRD graphs.

## 6.6 Experimental Validation of numerical simulation

In this study to experimentally validate the simulation, the bedplate sample, also known as the baseplate, utilized was constructed from S355JR rolled structural steel. The composition of this material is outlined in Table 1. It is extensively employed in various industries, particularly in applications related to oil and gas, as well as offshore wind turbines. Table 2 summarizes the chemical composition of the consumable electrode (with iron as the major component). This electrode primarily consists of austenite and ferrite phases, with the former having a negligible impact on the material properties. Consequently, there is no need to incorporate material phase transformation modeling in the numerical simulations.

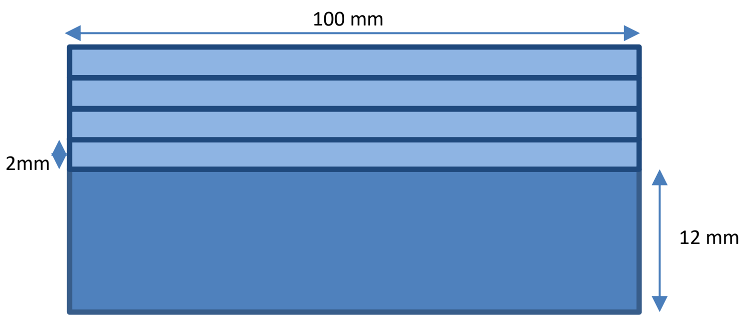


Figure 20 Schematic of WAAM model for validation

In the fabrication of the WAAM wall examined in this study[20], a welding wire with a diameter of 1.2 mm was utilized. The wire was fed at a speed of 10 m/min, while the welding torch travelled at a speed of 8.33 mm/s. The heat input for the welding process amounted to 2245.83 W. Additionally, a waiting time of 400 s was observed between successive layers to ensure that the deposited layer cooled down to a temperature below 50 °C before new layers were added (Ref 5). To aid the cooling process, a water-cooled aluminum backing plate was implemented.

*Table 2 Chemical composition of the S355JR baseplate (in wt.%)*

| **C** | **Mn** | **Si** | **P** | **S** | **N** | **Nb** |
|---|---|---|---|---|---|---|
| 0.24 | 1.60 | 0.55 | 0.045 | 0.045 | 0.009 | 0.003-0.100 |

Table 3 Chemical composition of the consumable electrode (in wt.%)

| C | Mn | Si | Cu | P | S |
|---|---|---|---|---|---|
| 0.08 | 1.50 | 0.92 | 0.16 | <0.040 | <0.035 |

For simulating the residual stress, a deposited wall with shape identical to that of reference 5 was constructed in ABAQUS as shown in Figure 15. The "element Birth technique" was used to simulate the deposition of material layer-by-layer. Each of the layer was built in 12s with 400 s of inter-cooling time between each layer. Hence, in the simulation, each layer consisted of 12 steps each of 1s time period.

Table 4 Parameter Table for Experimental Validation

| Symbol | Parameter | Value |
|---|---|---|
| Q | Heat Input | 2245.83W |
| V | Scanning speed | 8.33 mm/s |
| F | Feed rate | 10 m/min |
| f_f | Heat fraction coefficient in front ellipsoid | 0.6 |
| f_r | Heat fraction coefficient in rear ellipsoid | 1.4 |
| $c_f$ | Length of the front ellipsoid | 2 mm |
| $c_r$ | Length of the rear ellipsoid | 6 mm |
| a | Width of the ellipsoid | 3 mm |
| b | Depth of the ellipsoid | 2.5 mm |

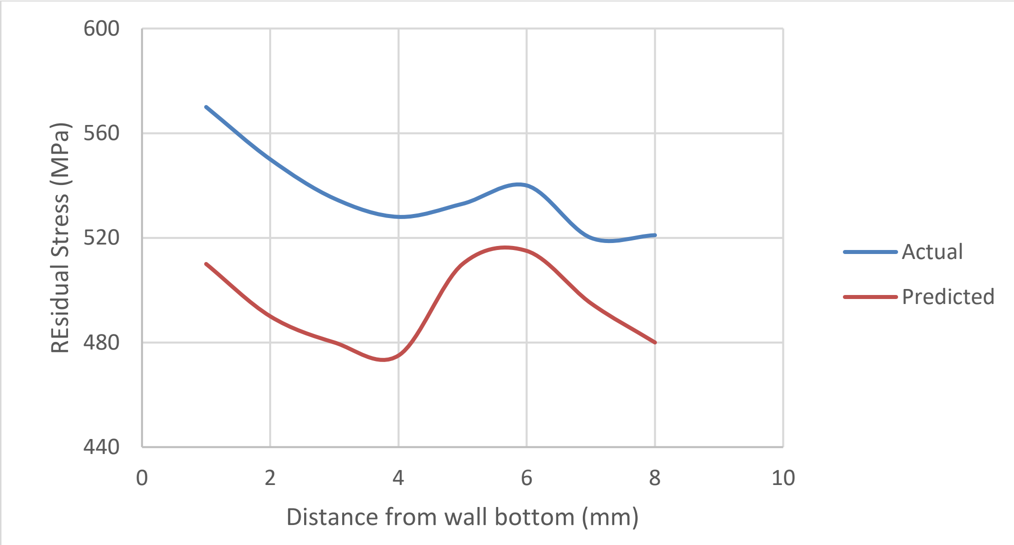


Figure 21 Comparison of simulated and experimental residual stress data

The obtained nodal temperature distribution, acquired through thermal analysis, serves as the predefined field in the mechanical model to predict residual stress. The residual or von Mises stress is then estimated along the Z-direction and compared to the actual residual stress documented in the paper as shown in the Figure 18. The cumulative percentage error was approximately 7.92%, which is reasonably acceptable considering the assumptions made during simulation and the difficulty in obtaining precise parameter values for the ellipsoid. As the material data was derived from literature, it is important to acknowledge that the actual behavior of the material may differ from the modeled behavior. Additionally, no tuning operation was conducted for convection coefficients and heat source parameters, which is typically performed in works related to WAAM simulation. Nevertheless, the proposed model provides a dependable prediction of residual stress with satisfactory accuracy, and further improvement can be achieved by better representing the actual material behavior and boundary conditions

## 6.7 Temperature Profile

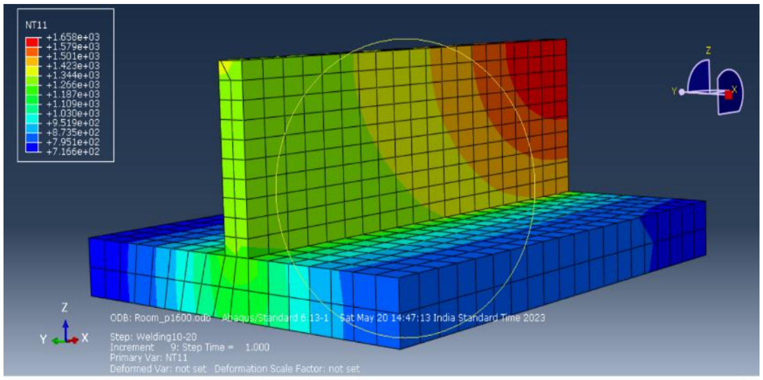


*Figure 22 Nodal temperature (℃) distribution on non-preheated sample*

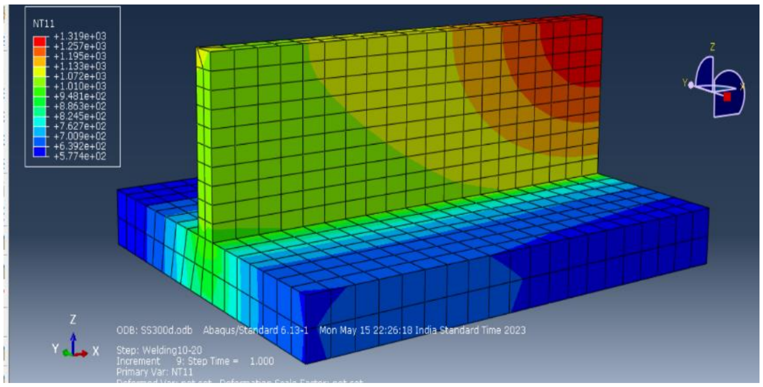


*Figure 23 Nodal Temperature (℃) distribution on preheated sample at 300 ℃*

Figure 19 and 20 above depict the Nodal temperature distribution during the final increment of the last step (Welding 10-20). The nodal temperature is generally higher for the non-preheated copper wall, as it requires more power for deposition (1600 W in the current case). In contrast, the preheated plate requires relatively less power for deposition (1000 W in the current case). However, when focusing solely on the preheated plate, as the base plate's preheating temperature increases, the temperature of the copper wall structure also increases, as illustrated in Figure 12.

Furthermore, when examining the temperature variation at a specific node throughout the welding process, it displays a consistent pattern of increasing and decreasing. This behavior is commonly observed in nodes of typical additive manufacturing components[20]. The temperature rises repeatedly due to the continuous deposition of material layers, while simultaneously experiencing temperature reductions due to convection and radiation. Figure 13 illustrates the typical temperature profile for a node located in the middle region of a non-preheated sample.

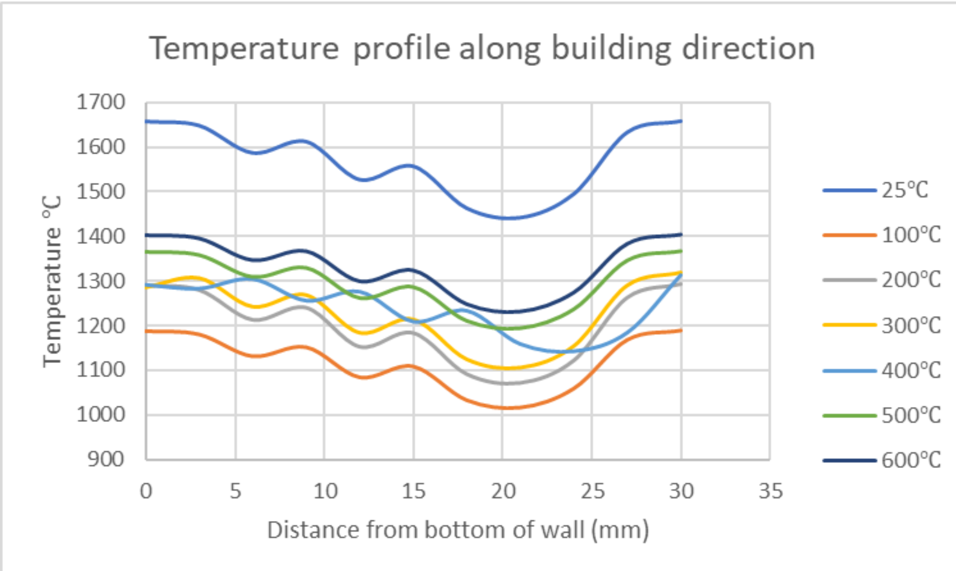


*Figure 24 Temperature variation on building direction for different samples*

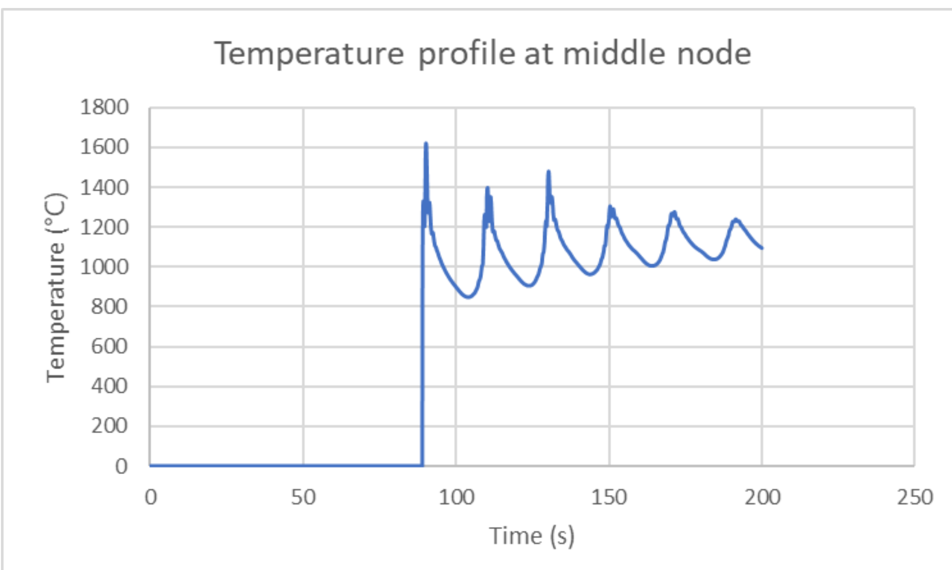


*Figure 25 Temperature Profile at node situated on the middle layer of deposition*

## 6.8 Residual Stress profile

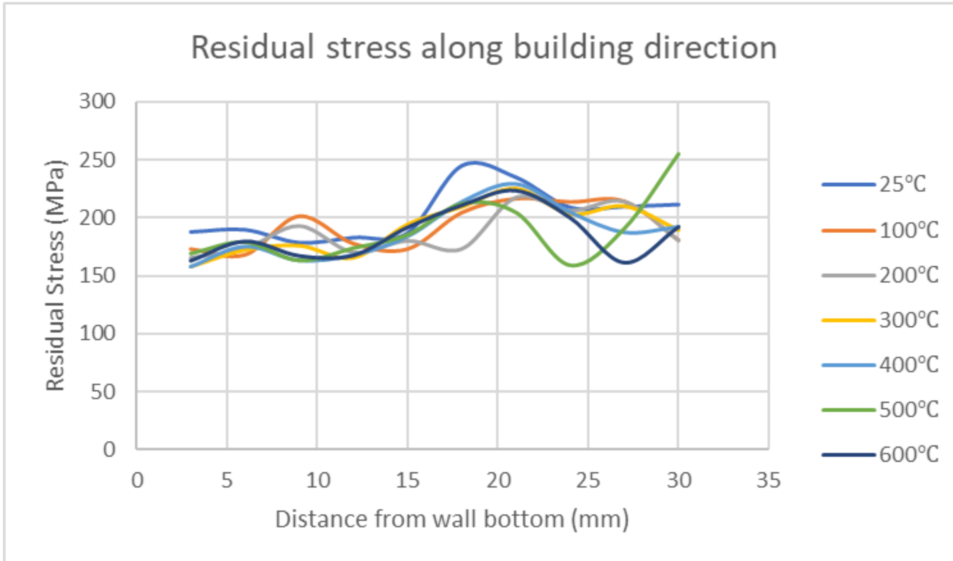


Figure 26 Residual stress profile along building direction

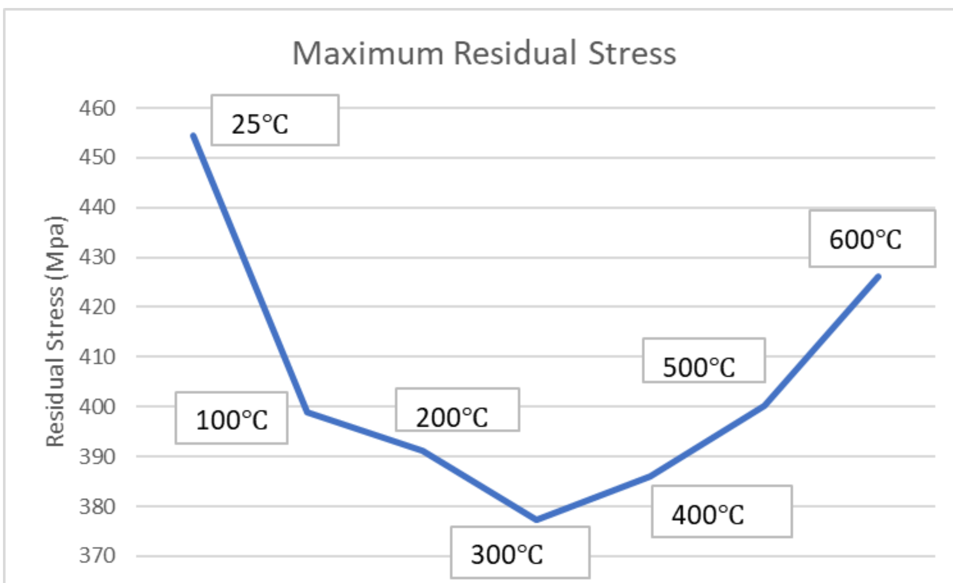


Figure 27 Maximum longitudinal residual stress at various temperatures

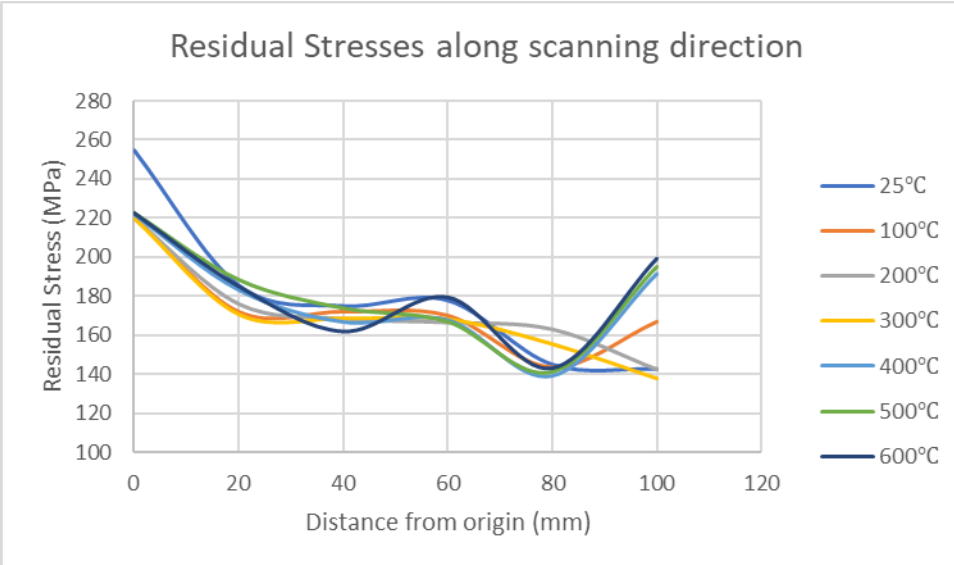


Figure 28 Residual stress along scanning direction at various temperature

The residual stress in the building direction for non-preheated sample is more compared to preheated sample. However, as the preheating temperature is increasing, the residual stresses are further increasing after certain temperature value. Excessive preheating of the base plate in wire arc additive manufacturing (WAAM) can lead to an increase in residual stresses within the component. This is because excessive preheating can result in a significant temperature difference between the base plate and the deposited material. When the heated material cools and solidifies, it undergoes thermal contraction. If this contraction is restricted or mismatched due to the excessive preheating, it can cause residual stresses to build up within the material. Furthermore, it affects the cooling rates of the deposited material. Rapid cooling or cooling at different rates across the component can lead to non-uniform thermal contraction and the generation of residual stresses. High temperatures during preheating can induce metallurgical changes within the base plate and deposited material, such as grain growth or phase transformations. These changes can introduce variations in material properties and result in localized stress concentrations. Excessive preheating may induce phase transformations or structural changes in the material. These transformations can be associated with volumetric changes that generate stress within the material as it cools and solidifies.

# CHAPTER 7: CONCLUSIONS AND FUTURE SCOPE

## 7.1 Conclusion

- Preheating the substrate before the deposition of material improves microstructure and mechanical properties.
- Due to preheating of the plate, lesser thermal gradients are formed, which helps in the formation of coarse and refined grains.
- Tensile strength of the preheated sample along scanning direction came about 280 MPa compared to 225 MPa of the non-preheated sample due to the presence of finer grains.
- Hardness of the preheated sample along scanning direction is 92 HV, which is more than the non-preheated sample having 85 HV.
- Coefficient of friction along the building direction for the preheated sample is 0.18 which is lesser than the non-preheated sample having a value of 0.27. Hence, the preheated sample has great frictional efficiency and wear resistance property.
- The numerical simulation is validated by comparing the residual stress value present in the literature and percentage error came about 7.92%
- Power requirement for non-preheated sample (1600W) is more than as compared to preheated sample (1000W).
- Preheating the substrate reduces the amount of residual stress induced in the material.
- The improvement in the residual stress is valid up to a certain temperature value. Above a certain temperature value, the residual stresses further increase.

## 7.2 Future Scope

- Further characterization techniques, such as EBSD (Electron Backscatter Diffraction) and tribology, can be performed on both the non-preheated and preheated samples to compare them and determine their suitability for different applications.

- The simulation can be validated with the self-conduct experimental results of either temperature profile, distortion, or residual stress.

- The presented simulation model can be fully automated with the help of python codes, which would eventually require a few lines of code to prepare simulation with required parameters.

- The present simulation can be extended for multi-pass and multi-material systems.

- The thermal fields obtained from the thermal analysis of the simulation can be used for the prediction of microstructure, which can help to optimize the material properties (since mechanical properties are dependent on the microstructure)

# CHAPTER 8: REFERENCES


[1] Y. Li, C. Su, and J. Zhu, “Comprehensive review of wire arc additive manufacturing: Hardware system, physical process, monitoring, property characterization, application and future prospects,” *Results Eng.*, vol. 13, no. September 2021, p. 100330, 2022, doi: 10.1016/j.rineng.2021.100330.

[2] J. Baby and M. Amirthalingam, “Microstructural development during wire arc additive manufacturing of copper-based components,” *Weld. World*, vol. 64, no. 2, pp. 395–405, Feb. 2020, doi: 10.1007/s40194-019-00840-y.

[3] S. Yadav, C. P. Paul, A. N. Jinoop, A. K. Rai, and K. S. Bindra, “Laser Directed Energy Deposition based Additive Manufacturing of Copper: Process Development and Material Characterizations,” *J. Manuf. Process.*, vol. 58, pp. 984–997, Oct. 2020, doi: 10.1016/j.jmapro.2020.09.008.

[4] R. Guschlbauer, S. Momeni, F. Osmanlic, and C. Körner, “Process development of 99.95% pure copper processed via selective electron beam melting and its mechanical and physical properties,” *Mater. Charact.*, vol. 143, pp. 163–170, Sep. 2018, doi: 10.1016/j.matchar.2018.04.009.

[5] T. T. Ikeshoji, K. Nakamura, M. Yonehara, K. Imai, and H. Kyogoku, “Selective Laser Melting of Pure Copper,” *JOM*, vol. 70, no. 3, pp. 396–400, Mar. 2018, doi: 10.1007/s11837-017-2695-x.

[6] M. Colopi, A. G. Demir, L. Caprio, and B. Previtali, “Limits and solutions in processing pure Cu via selective laser melting using a high-power single-mode fiber laser,” *Int. J. Adv. Manuf. Technol.*, vol. 104, no. 5–8, pp. 2473–2486, Oct. 2019, doi: 10.1007/s00170-019-04015-3.

[7] F. Montevecchi, G. Venturini, A. Scippa, and G. Campatelli, “Finite Element Modelling of Wire-arc-additive-manufacturing Process,” in *Procedia CIRP*, Elsevier B.V., 2016, pp. 109–114. doi: 10.1016/j.procir.2016.08.024.

[8] Y. Liu *et al.*, “Additive manufacturing of high strength copper alloy with heterogeneous grain structure through laser powder bed fusion,” *Acta Mater.*, vol. 220, Nov. 2021, doi: 10.1016/j.actamat.2021.117311.

[9] S. Yadav, C. P. Paul, A. N. Jinoop, S. K. Nayak, A. K. Rai, and K. S. Bindra, “EFFECT OF PROCESS PARAMETERS ON LASER DIRECTED ENERGY DEPOSITION OF COPPER,” 2019. [Online]. Available: http://asmedigitalcollection.asme.org/GTINDIA/proceedings-pdf/GTINDIA2019/83532/V002T10A004/6476592/v002t10a004-gtindia2019-2453.pdf

[10] B. Dong, “Fabricating copper-rich Cu-Al binary alloy by wire-arc additive Fabricating copper-rich Cu-Al binary alloy by wire-arc additive manufacturing manufacturing.” [Online]. Available: https://ro.uow.edu.au/theses1

[11] P. S. Deshmukh, K. Tomar, G. D. Sathiaraj, and I. A. Palani, “Optimum strength and ductility of pure copper fabricated by Wire Arc Additive Manufacturing,” *Manuf. Lett.*, vol. 33, pp. 24–28, Aug. 2022, doi: 10.1016/j.mfglet.2022.06.005.

[12] T. I. El-Wardany, Y. She, V. N. Jagdale, J. K. Garofano, J. J. Liou, and W. R. Schmidt, “Challenges in Three-Dimensional Printing of High-Conductivity Copper,” *J. Electron. Packag. Trans. ASME*, vol. 140, no. 2, Jun. 2018, doi: 10.1115/1.4039974.

[13] S. W. Williams, A. Rashid, G. Pardal, and & L. Quintino, *WIRE AND ARC ADDITIVE MANUFACTURE OF HIGHLY CONDUCTING PURE COPPER*.

[14] J. Goldak, A. Chakravarti, and M. Bibby, “A New Finite Element Model for Welding Heat Sources.”

[15] P. Singh, R. M.Singari, and R. S. Mishra, “A review of study on modeling and simulation of additive manufacturing processes,” *Mater. Today Proc.*, vol. 56, pp. 3594–3603, Jan. 2022, doi: 10.1016/j.matpr.2021.12.057.

[16] R. Geng, J. Du, Z. Wei, and N. Ma, “Multiscale modelling of microstructure, micro-segregation, and local mechanical properties of Al-Cu alloys in wire and arc additive manufacturing,” *Addit. Manuf.*, vol. 36, Dec. 2020, doi: 10.1016/j.addma.2020.101735.

[17] N. An, G. Yang, K. Yang, J. Wang, M. Li, and J. Zhou, “Implementation of Abaqus user subroutines and plugin for thermal analysis of powder-bed electron-beam-melting additive manufacturing process,” *Mater. Today Commun.*, vol. 27, Jun. 2021, doi: 10.1016/j.mtcomm.2021.102307.

[18] E. A. Bonifaz and J. S. Palomeque, “A mechanical model in wire + Arc additive manufacturing process,” *Prog. Addit. Manuf.*, vol. 5, no. 2, pp. 163–169, Jun. 2020, doi: 10.1007/s40964-020-00112-y.

[19] R. Tangestani, G. H. Farrahi, M. Shishegar, B. P. Aghchehkandi, S. Ganguly, and A. Mehmanparast, “Effects of Vertical and Pinch Rolling on Residual Stress Distributions in Wire and Arc Additively Manufactured Components,” *J. Mater. Eng. Perform.*, vol. 29, no. 4, pp. 2073–2084, Apr. 2020, doi: 10.1007/s11665-020-04767-0.

[20] J. Ding *et al.*, “Thermo-mechanical analysis of Wire and Arc Additive Layer Manufacturing process on large multi-layer parts,” *Comput. Mater. Sci.*, vol. 50, no. 12, pp. 3315–3322, 2011, doi: 10.1016/j.commatsci.2011.06.023.

[21] K. V. Chauhan and S. K. Rawal, “A Review Paper on Tribological and Mechanical Properties of Ternary Nitride based Coatings,” *Procedia Technol.*, vol. 14, pp. 430–437, 2014, doi: 10.1016/j.protcy.2014.08.055.

[22] ABAQUS/CAE user’s manual

[23] https://www.symmetryelectronics.com/blog/defining-additive-manufacturing/ (last accessed on 28/05/2023 at 11.06 AM)

[24] https://www.researchgate.net/figure/Schematic-illustration-of-the-wire-and-arc-additive-manufacturing-WAAM-process-20_fig5_350012077 (last accessed on 28/05/2023 at 11.10 AM)

[25] https://images.app.goo.gl/seMKqw9JgCGEbxkS7 (last accessed on 28/05/2023 at 11.12 AM)

[26] https://medium.com/@sriram_83285/a-new-approach-to-wire-arc-based-additive-manufacturing-process-c7b0fb15b481 (last accessed on 28/05/2023 at 11.15 AM)